Characterization of C_4H in the $A^2\Pi$ and $X^2\Sigma^+$ states by double resonance four-wave mixing

Fabio J. Mazzotti, Ranjini Raghunandan, Aaseef Muhammed Esmail, Marek Tulej, and John P. Maier'

Citation: The Journal of Chemical Physics **134**, 164303 (2011); doi: 10.1063/1.3578188
View online: http://dx.doi.org/10.1063/1.3578188
View Table of Contents: http://aip.scitation.org/toc/jcp/134/16
Published by the American Institute of Physics

Characterization of C_4H in the $A^2\Pi$ and $X^2\Sigma^+$ states by double resonance four-wave mixing

Fabio J. Mazzotti,[1] Ranjini Raghunandan,[1] Aaseef Muhammed Esmail,[1] Marek Tulej,[2] and John P. Maier[1,a)]

[1]*Department of Chemistry, University of Basel, Klingelbergstrasse 80, CH-4056, Switzerland*
[2]*Institute of Physics, Planetology and Space Research, University of Bern, Sidlerstrasse 5, CH-3012 Bern, Switzerland*

(Received 13 December 2010; accepted 17 March 2011; published online 22 April 2011)

The $B^2\Pi - X^2\Sigma^+$ electronic spectrum of C_4H has been studied by degenerate and double resonance four-wave mixing. The technique identifies vibrational levels in the $X^2\Sigma^+$ ground state. Its sensitivity and unique characteristics permit detection of new levels. The $A^2\Pi$ state lying 222 cm^{-1} above the $X^2\Sigma$ ground state is also observed, confirming the analysis from anion photoelectron spectroscopy but with improved accuracy. Vibrational level determination in the $A^2\Pi$ electronic manifold up to 700 cm^{-1} above v = 0 is made. A Renner–Teller analysis is carried out for the two lowest bending modes v_6 and v_7 in the $A^2\Pi$ state by diagonalization of the effective Hamiltonian matrix. The Renner–Teller parameters ϵ_6, ϵ_7, and ϵ_{67}, the vibrations ω_6 and ω_7 and the spin–orbit coupling constant A_{so} are determined. © *2011 American Institute of Physics*. [doi:10.1063/1.3578188]

I. INTRODUCTION

The linear butadiynyl C_4H was identified in the carbon rich star IRC+10 216 in 1978 (Ref. 1) as well as in dense clouds.[2,3] Five years after its detection, the laboratory spectrum was reported by microwave spectroscopy[4] confirming its existence in the interstellar medium.[5,6] C_4D was later observed by radio astronomy.[7] Since then, the electronic structure of the C_4H radical has been of interest from a spectroscopic point of view. A study of the $B^2\Pi - X^2\Sigma^+$ electronic transition by laser induced fluorescence yielded the origin at around 24 033 cm^{-1} and provided a tentative assignment of the two lowest bending modes in the excited state.[8] The photoelectron spectrum of the C_4H^- anion located the $A^2\Pi$ state about 213 cm^{-1} above the $X^2\Sigma^+$ ground state.[9] The spectroscopy of the radical is challenging because of the closely lying $X^2\Sigma^+$ and $A^2\Pi$ states. The order of the electronic states is reversed for the higher members of the $C_{2n}H$ species.

The Renner–Teller (R–T) effective Hamiltonian relevant to a linear triatomic molecule in a $^2\Pi$ electronic state with a single degenerate bending vibration is known.[10] The formalism for a tetraatomic with two bending modes has been quantified in the case of HC_2S recorded by microwave spectroscopy,[11] and a model for polyatomic linear molecules sketched.[12] C_4H in the $B^2\Pi$ excited state has been studied with the same Hamiltonian matrix.[8]

The C_4H radical was also detected by degenerate four-wave mixing.[13] The measurements proved the technique to be sensitive and selective when combined with a supersonic slit-jet discharge source. In the present study, the experimental determination of the energy above the ground state of the vibronic levels is possible with the double resonance four-wave mixing technique, without the ambiguity of hot bands. The assignment is aided by a theoretical treatment of the R–T and spin–orbit interactions derived previously for a tetraatomic molecule.[11]

II. EXPERIMENTAL

A 3 × 0.3 mm slit was used for the supersonic expansion and a pulse of 1100–1800 kV was applied to 1% acetylene in argon (7–10 bar) for production of the C_4H radical. The discharge was generated in the region between the electrodes. The ground plate was positioned at the output of the multichannel body and the two cathodes just before the expansion in vacuum.[14] The high-voltage pulse duration was 0.3–1.0 μs for the degenerate four-wave mixing (DFWM) measurements but 0.3–3 μs for the two-color resonant four-wave mixing, because of increased selectivity. A longer discharge pulse in DFWM resulted in a spectrum with predominant features originating from the C_3 $A^1\Pi_u - X^1\Sigma_g^+$ electronic system.[13] The delay between the valve and the discharge trigger was 1200–2100 μs and 5–7 μs between the laser and the discharge, depending on the distance of the laser beam to the slit.

Pulses of 7 ns duration were generated by dye lasers pumped by the 355 nm output of Nd:YAG lasers with linewidths of 0.06 cm^{-1} (double grating) and 0.15 cm^{-1} (or 0.05 cm^{-1} with an intracavity etalon). A wavemeter provided the calibration. The signal beam travels through collimating lenses set on a long pathlength before reaching a photomultiplier.[15] The data were averaged over 40 laser shots and 0.06 cm^{-1} steps were used for the scans.

The degenerate scan allowed selection and detection of specific transitions of C_4H for the pump laser. Double resonance scans were made at higher or lower energy relative to the pump frequency and gave access to the allowed transitions

a)Author to whom correspondence should be addressed. Electronic mail: j.p.maier@unibas.ch.

resonant with the pump photons. By increasing the intensity of the probe or the pump lasers, it is possible to access weak vibronic transitions.

The experimental setup was modified compared to the previous arrangement to permit fast switching between the degenerate and double-resonance configuration. This was achieved by using a 50% beamsplitter so that the two probes traveled through the same path. The difference in alignment induced by the wavelength difference between pump and probe as well as index of refraction variation with frequency of the beamsplitter was negligible and no realignment was necessary throughout the whole range of the dyes used.

The C_4H radical was probed close to the slit. In this region, the observed rotational temperature of approximately 100 K combined with nonlinear four-wave mixing effects produces an intensity enhancement of the R bandhead which gives rise to the observation of even the weakest vibronic bands. Observation of transitions originating from the ground electronic state in vibrationally excited levels shows that the vibrational temperature is a few hundreds K.

The stimulated emission pumping (SEP) scheme (transitions resonant with a common upper state) leads to unambiguous determination of the vibrational/electronic energy levels above the ground state provided that the pump laser is tuned to an origin band of a given electronic transition. A scan of the probe to the lower energy range will reveal the ground state levels as shown in Fig. 1(a). However, if the pump is tuned to a vibronic excited state, an ambiguity arises [Fig. 1(b)] even if the probe frequency is less than the one of the pump. The resonant transition can bear a common state in the upper or the lower manifold as well.

In case the origin of an electronic system is not readily assigned and hot bands are present, it is possible to scan first in a degenerate fashion to obtain the transitions (including hot bands or excited states) and second to map the ground and excited state levels with a series of double-resonance spectra by sitting on each and every transition without realigning the optics. This scheme of operation is similar to two-color laser induced fluorescence.

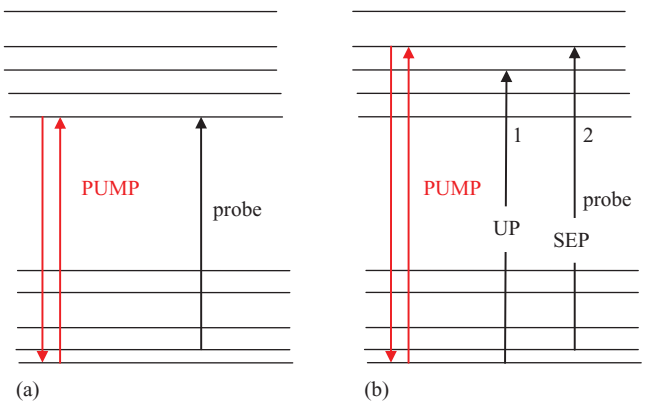

FIG. 1. Two-color resonant four-wave mixing with pump frequency tuned either to the origin (a) or to an excited state (b) of an electronic transition. A probe lower in frequency is considered. The levels detected map out the ground state manifold in (a) while levels in the excited (1) and the ground state (2) are resonant in (b).

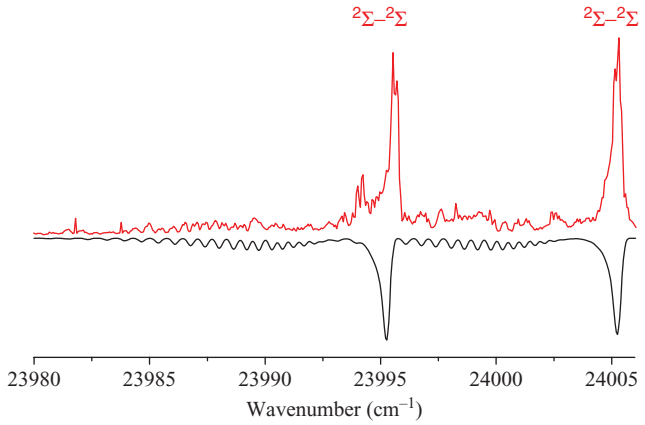

FIG. 2. Degenerate four-wave mixing scan of the newly detected $^2\Sigma^+ - ^2\Sigma^+$ bands of C_4H. The experimental spectrum (top) is matched against the simulation (inverted trace) at a temperature of 40 K.

III. RESULTS AND DISCUSSION

A. Single color

Most of the bands observed previously using laser induced fluorescence[8] were also detected with DFWM, some of them being concealed by the presence of strong C_3 $A^1\Pi_u - X^1\Sigma_g^+$ hot bands. Among these, the $B^2\Pi - X^2\Sigma^+$ origin band of C_4H (Ref. 8) was not measured by DFWM because of the spectral congestion and weak signals. However, two relatively intense transitions were recorded with R bandheads at 23 995 and 24 005 cm^{-1} (Fig. 2). The latter was used as a pump transition, in addition to the $^2\Sigma^+ - X^2\Sigma^+$ band[8] at 24 493 cm^{-1} (labeled J in Ref. 8) and the origin of the $B^2\Pi_{3/2} - X^2\Sigma^+$ transition at 24 023 cm^{-1}. The symmetries of the levels involved are of $^2\Sigma$ character.

B. Double resonance

The double resonance method has increased selectivity compared to the degenerate case. The previously detected[8] $B^2\Pi - X^2\Sigma^+$ transition overlapping with a hot band of the $A^1\Pi_u - X^1\Sigma_g^+$ electronic transition of C_3 is readily observed in the two-color configuration when pumping on the J feature at 24 493 cm^{-1}, which originates from the $X^2\Sigma^+$ ground state and accedes to a vibration located 470 cm^{-1} above and within the $B^2\Pi$ state. Consequently, the spectral region can be scanned by pumping on the $B^2\Pi - X^2\Sigma^+$ origin band: levels lying above the ground state will be detected with lower probe frequency and the excited states with higher one. The technique provides rotationally resolved spectra (Fig. 3). The recording was made by setting the pump frequency at 24 493 cm^{-1} (J feature) and are interpreted as follows. Two $^2\Sigma - ^2\Sigma$ transitions are visible, one is the pump transition and the other is detected 234 cm^{-1} red-shifted; more interestingly a third is identified as $^2\Pi - ^2\Sigma$ lying 262 cm^{-1} toward lower energy. The resolved P lines and R branches of the latter transition allow an estimate of the spin–orbit splitting in the upper state, inferred from the separation between the bandheads.

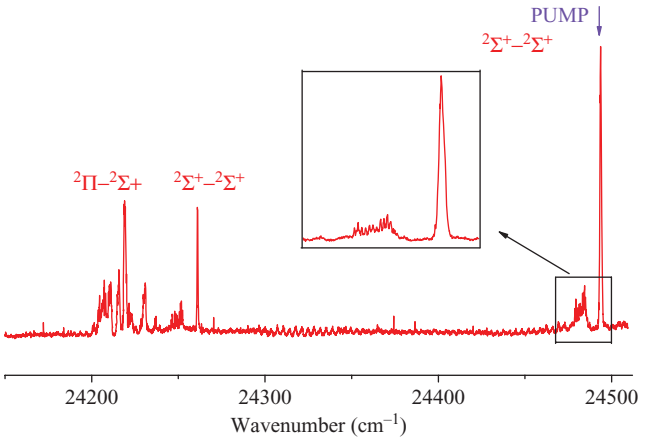

FIG. 3. Rotationally resolved two-color four-wave mixing spectrum of C_4H with the pump frequency resonant with the "J" $B^2\Sigma - X^2\Sigma^+$ transition (Ref. 8) at 24 493 cm^{-1}. Three bands are visible: two $B^2\Sigma^+ - X^2\Sigma^+$ and one $B^2\Pi - X^2\Sigma^+$. The oscillations around 24 300 cm^{-1} are due to minute spatial drifts of the probe beam while scanning the wavelength.

The $^2\Pi - ^2\Sigma$ transition shown in Fig. 4 was recorded by setting the pump wavelength on the R head of the "J" band[8] and scanning in the vicinity of 24 200 cm^{-1}. Because of the higher rotational temperature achieved in the discharge, the trace displays a succession of band heads as well as the simulations. The spectroscopic constants involved in the pump transition were taken from Ref. 8. The rotational lines were calculated with the PGOPHER program[16] and a home-made software simulated the double-resonance traces shown as middle trace in Fig. 4. The small mismatch in the line positions is due to the fact that the rotational constant in the excited state could not be perfectly fitted. The simulation of a two-color spectrum is beyond the scope of this paper but has been undertaken previously for $^2\Pi - ^2\Pi$ transitions in the HC_2S radical.[17]

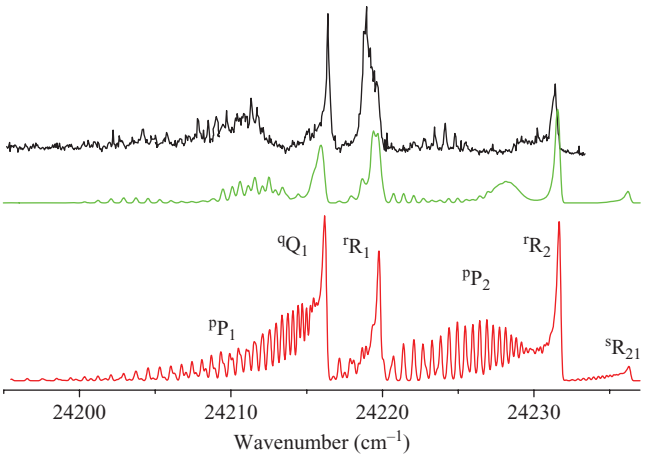

FIG. 4. Double resonance spectrum of the $B^2\Pi - X^2\Sigma^+$ transition of C_4H with pump frequency set on the $B^2\Sigma - X^2\Sigma^+$ band at 24 493 cm^{-1}. The bottom trace is the simulation of the absorption squared. The experimental spectrum shows a selected subset of J lines in each of the P, Q, R bands and is reproduced in the middle trace by a two-color simulation. The mismatch between the spectra is due to the use of approximate spectroscopic constants in the upper state.

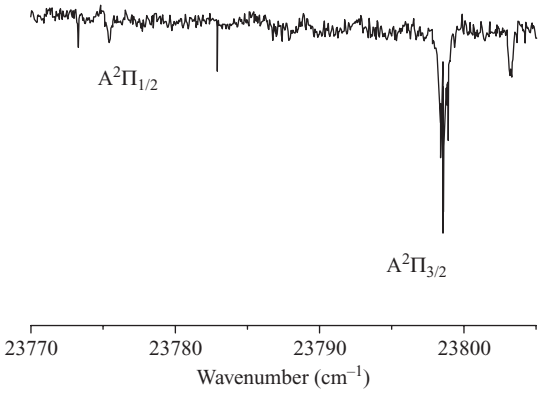

FIG. 5. Two-color four-wave mixing spectrum of the C_4H $B^2\Pi - X^2\Sigma^+$ transition with pump laser set on the $B^2\Pi_{3/2} - X^2\Sigma^+$ origin band. The two peaks labeled on the plot correspond to the two spin–orbit components of the $A^2\Pi$ state located 213 cm^{-1} above the $X^2\Sigma^+$ by the photoelectron recordings (Ref. 9).

C. $A^2\Pi$ state spin–orbit splitting

Figure 5 shows a two-color scan of the C_4H $B^2\Pi - X^2\Sigma$ system with pump on the $B^2\Pi_{3/2} - X^2\Sigma^+$ transition. The frequency was precisely measured by setting the pump on the J band and scanning the probe toward lower frequencies, thus confirming the previous spectroscopic data.[8] The intense peak corresponds to the $A^2\Pi_{3/2}$ level while the weaker one to $A^2\Pi_{1/2}$. A photoelectron experiment located the $A^2\Pi$ state at 213 cm^{-1},[9] close to the one detected by double resonance spectroscopy at 222 cm^{-1}. No rotational lines were resolved for this state while scanning the probe laser, because of the small signals and the relatively large laser power required for the detection of the R bandheads causing saturation in the four-wave-mixing technique. At 246 cm^{-1}, a second level is detected and identified as belonging to the $\Omega = 1/2$ manifold, resulting in a separation of -28 cm^{-1} between the spin–orbit (s–o) components. It is interesting to observe that even the weak $B^2\Pi_{3/2} - A^2\Pi_{1/2}$ transition is detected. A similar effect was observed in the $d^3\Pi_g - a^3\Pi_u$ system of C_2 by two-color four-wave-mixing whenever the intensity of the pump laser was increased.[15] In the present case, the probe frequency is set on the less intense $B^2\Pi_{3/2} - A^2\Pi_{1/2}$ transition and the pump on the strong $B^2\Pi_{3/2} - X^2\Sigma^+$ in a SEP fashion. The measured s–o splitting in the $A^2\Pi$ state is consistent with an empirical value based on the following observations. The $B^2\Pi$ of C_4H and $^2\Pi$ states of C_6H arise from the singly unoccupied orbital configurations $1\pi^3$ and $2\pi^3$, respectively. These two electronic states have a similar s-o constant, ~ -16 cm^{-1}.[8,18] Similarly, the C_4H $A^2\Pi$ and C_6H $X^2\Pi$ states should have comparable splitting, ≈ -25 cm^{-1}, because they arise from $2\pi^3$ and $3\pi^3$ open shell configurations. This alternating behavior is similar to that described in the theoretical calculations of the s–o splitting of the HC_nS series.[19] The A_{so} parameter was determined via the R–T analysis.

D. Renner–Teller analysis: Effective Hamiltonian

The R–T analysis was carried out as in Ref. 20, using an effective Hamiltonian diagonalization. The matrix

coefficients were calculated according to previously determined formulas[21] for any level of vibronic symmetry $K = |l_7 + l_6 + \Lambda|$ (l_7 and l_6 are the vibronic angular momenta associated with the two degenerate vibrations and Λ the electronic angular momentum). l_7 was varied from $-v_7$ to v_7 while Σ and Λ took all possible combinations of $\pm 1/2$ and ± 1 values, respectively. The off-diagonal terms related to ϵ_6 and ϵ_7 are nonzero within block matrices obeying $\Delta v_7 = 0, \pm 2$ according to the formulas given in Ref. 21. The R–T interaction related to the ϵ_{67} parameter has nonvanishing terms in the Hamiltonian for $\Delta v_7 = \pm 1, \Delta l_7 = -1, \Delta v_6 = \pm 1, \Delta l_6 = -1, \Delta\Lambda = -2$ and complex conjugate. The s–o and the R–T interaction for the two lowest bending vibrations were taken into consideration. Terms were taken up to $v = 4$ and $|P| \leq 2.5$ resulting in a block-diagonal square matrix of size 568 × 568 (largest block size is 105 × 105) expressed in a $|v_7, v_6, l_7, l_6, \Lambda, \Sigma\rangle$ basis set. The assignment was made by choosing the $|v_7, v_6, l_7, l_6, \Lambda, \Sigma\rangle$ element which had the highest coefficient (reported in Table I) of the eigenvector basis expansion. This formalism, in principle only valid for a tetraatomic molecule, is used for C_4H as previously done for the excited state.[8] The quartic terms of the potential energy curve relatively to a bending angle are contained in the anharmonic terms of the model which were not considered.

The parameters ϵ_6, ϵ_7, ϵ_{67}, ω_6, ω_7, and A_{so} were fitted and a vibrational energy level assignment could be inferred from the experimental data (Table I and Fig. 6). The R–T parameters were initially set equal to the ones given in Ref. 8 based on the assumption that the skeletal *cis* and *trans* C–C–C–C bending of C_4H in the $B^2\Pi$ and $A^2\Pi$ states have similar characteristics. However, the experimental line list was not reproduced satisfactorily. A higher $|\epsilon_6|$ value is required in order to reproduce all the observed levels, as explained below. A least squares fit was performed by matching the calculated levels with the experimental findings (12 levels included), one of them being a R–T mode lying 122 cm^{-1} below the $A^2\Pi$ state. This procedure led to a satisfactory fit of the levels of higher energy. An average residual error of around 3.6 cm^{-1} (per level) was achieved. The results of the R–T fit are summarized in Table II, along with the root mean square (rms) value, found to be slightly better than the one obtained via laser-induced fluorescence measurements on C_3N with one less varied parameter.[20] The signs of the R–T parameters are ambiguous and were inferred from the previous analysis of the $B^2\Pi$ excited electronic state.[8] The number of parameters included in the fit was purposely kept small (5) in view of the limited experimental levels available. Possible inclusion of Sears resonance,[21] as well as anharmonicities was thus not taken into account and the simple model of Ref. 8 was preferred instead, as the lowest vibronic levels were to be reproduced. On the basis of the experimental linelist, several of the energy levels are assigned to vibrations in the electronic $X^2\Sigma^+$ ground state. The R–T parameters differ somewhat from those given for the $B^2\Pi$ excited state of C_4H in Ref. 8. The large $\epsilon_6 = -0.99(1)$ indicates that the potential surface has an energy minimum in a nonlinear geometry. A complete active space SCF calculation carried out by constraining a linear geometry for C_4H leads to a large splitting for the v_6 mode[22] and might confirm this; furthermore the molecule is quasilinear for this bending vibration in the excited state.[8] The calculations indicate that the linear configuration is a local energy minimum.[22] More precisely, the vibrational harmonic *ab initio* calculations show a large splitting (441–2007 cm^{-1})[22] for the two R–T components associated with the v_6 bending vibration. This results in $|\epsilon_6| \approx 0.90$, which is close to the value given in Table II. As reported in Table I, there is a vibrationally excited mode resulting from the diagonalization which lies below the $A^2\Pi$ state, at approximately -122 cm^{-1} with a $^2\Sigma$ character. This corresponds to the observations made by anion photoelectron spectroscopy for which a level at approximately ~ -125 cm^{-1} is detected.[9] The analysis indicates that it is a combination of the 7_1 vibrational state mixed with $7_1 6_2$, $7_1 6_4$ and more weakly with $7_3 6_0$, $7_3 6_2$,and $7_3 6_4$ because of the relatively high R–T parameter ϵ_6.

This effect is depicted by the energy level diagram shown in Fig. 7 for a small to large R–T coupling parameter ϵ_6. The variation of the energy levels with large ϵ_6 shows that the $v = 0$ level splits into a second component (at $\epsilon_6 \approx -0.95$) 214 cm^{-1} higher in energy. At $\epsilon_6 \approx -0.99$ both components

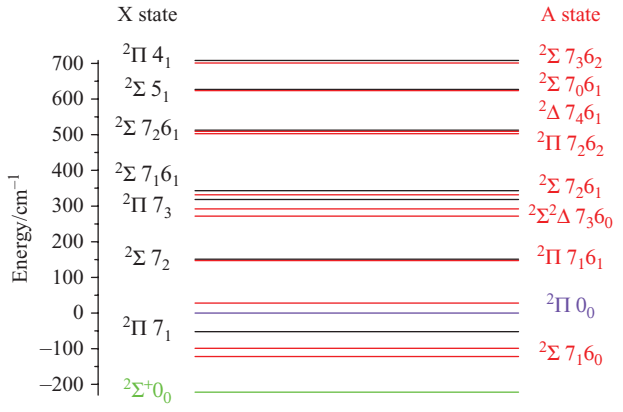

FIG. 6. Energy level diagram for C_4H showing the vibronic levels detected by two-color stimulated emission pumping resonant four-wave mixing along with their assignments (Table I). Not all levels given in Table I are shown.

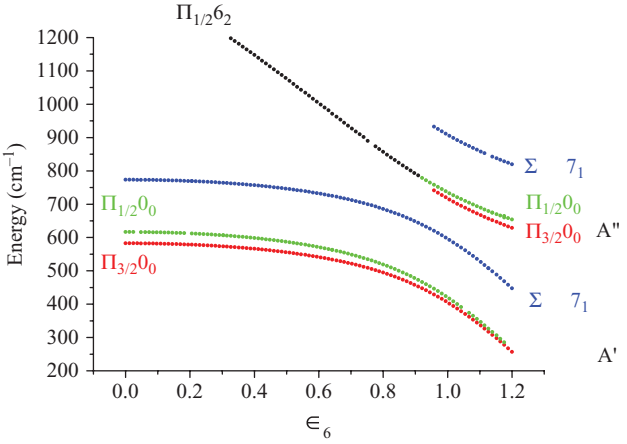

FIG. 7. Energy level dependence on ϵ_6 with $\epsilon_7 = -0.1$, $\epsilon_{67} = 0$. The $A^2\Pi$ $v = 0$ level starts to split for $\epsilon_6 \approx -0.95$. The higher energy component is significantly mixed with the 6_2 state. Symmetries in the C_s point group are indicated on the right.

TABLE I. Experimental and theoretical data given in cm^{-1}. The assignment $|v_7, v_6, l_7, l_6, \Lambda, \Sigma\rangle$ is made using the largest coefficient η obtained in the $|v_7, v_6, l_7, l_6, \Lambda, \Sigma\rangle$ basis expansion.

K	E (cm^{-1})[a]	v_6	v_7	l_7	P	η[b]	Calculated[c]	Observed[d]	Residuals[e]	Calculated[f]	Observed[g]	Assignment[h]
1.00	394.80	0	0	0	1.50	−0.75	−314.6			−92.8		
1.00	414.77	0	0	0	0.50	0.71	−294.6			−72.8		
0.00	439.96	1	0	0	0.50	0.62	−269.4			−47.6		
								−221.8			0	$X^2\Sigma^+$
								−212.5			9.3	
								−202.1			19.7	
								−195.2			26.6	
								−135.1			86.7	
								−126.6			95.2	
								−123.9			97.9	
0.00	587.62	0	1	−1	0.50	0.71	−121.8	−121.8	0.0	100.0	100	$A\ 7_1 6_0$
2.00	592.23	0	1	1	1.50	0.65	−117.2			104.6		
								−109.1			112.7	
								−104.3			117.5	
0.00	609.90	0	1	1	0.50	−0.68	−99.5	−98.8	0.7	122.3	123	$A\ 7_1 6_0$
								−89.5			132.3	
1.00	626.08	1	1	1	1.50	0.6	−83.3	−85.8		138.5	136	
1.00	627.13	1	1	1	0.50	−0.59	−82.3			139.5		
								−77.3			144.5	
								−70.7			151.1	
								−65.4			156.4	
2.00	655.90	1	0	0	2.50	0.75	−53.5	−51.9	1.6	168.3	169.9	$X\ 7_1$
2.00	676.59	1	0	0	1.50	−0.73	−32.8			189.0		
1.00	709.40	0	0	0	1.50	0.6	0.0	0.0	0.0	221.8	221.8	$A^2\Pi_{3/2}$
								4.9			226.7	
1.00	733.21	0	0	0	0.50	−0.65	23.8	28.1	4.3	245.6	249.9	$A^2\Pi_{1/2}$
1.00	767.38	0	2	0	1.50	−0.66	58.0			279.8		
3.00	769.20	0	2	2	2.50	−0.59	59.8			281.6		
1.00	778.08	0	2	2	0.50	−0.53	68.7			290.5		
1.00	791.70	0	2	0	0.50	0.49	82.3			304.1		
1.00	803.22	0	2	2	1.50	0.67	93.8			315.6		
0.00	811.79	1	2	0	0.50	0.56	102.4			324.2		
2.00	812.85	1	2	2	2.50	0.58	103.5			325.3		
2.00	814.86	1	2	2	1.50	−0.56	105.5			327.3		
3.00	842.73	2	0	0	2.50	0.57	133.3			355.1		
1.00	848.15	1	1	−1	1.50	−0.74	138.8	147.4	8.6	360.6	369.2	$A\ 6_1 7_1$
								150.9			372.7	$X\ 7_2$
								156.0			377.8	
1.00	868.57	1	1	−1	0.50	−0.71	159.2			381.0		
3.00	889.32	1	1	1	2.50	0.59	179.9			401.7		
0.00	892.22	0	1	−1	0.50	0.56	182.8			404.6		
2.00	900.09	0	1	1	2.50	0.58	190.7			412.5		
0.00	921.74	0	1	1	0.50	0.62	212.3			434.1		
2.00	922.76	0	1	1	1.50	−0.63	213.4			435.2		
2.00	948.32	0	3	1	2.50	0.61	238.9			460.7		
0.00	962.03	0	3	−1	0.50	−0.62	252.6			474.4		
2.00	963.36	0	3	1	1.50	0.55	254.0			475.8		
2.00	980.62	0	3	3	1.50	−0.67	271.2	269.3		493.4	491.1	
0.00	984.54	0	3	1	0.50	0.59	275.1	271.8	−3.3	496.9	493.6	$A\ 6_0 7_3$
								281.3			503.1	
2.00	996.59	0	3	3	2.50	−0.65	287.2	291.9	4.7	509.0	513.7	$A\ 6_0 7_3$
1.00	1000.65	1	3	1	1.50	−0.55	291.3			513.1		
1.00	1001.59	1	3	1	0.50	0.54	292.2			514.0		
3.00	1006.22	1	3	3	2.50	0.55	296.8			518.6		
2.00	1017.96	2	1	−1	2.50	−0.56	308.6			530.4		
								318.6			540.4	$X\ 7_3$
								323.0			544.8	
2.00	1034.46	2	1	−1	1.50	0.57	325.1			546.9		

TABLE I. (*Continued*)

K	E (cm^{-1})[a]	v_6	v_7	l_7	P	η[b]	Calculated[c]	Observed[d]	Residuals[e]	Calculated[f]	Observed[g]	Assignment[h]
0.00	1039.58	1	2	−2	0.50	−0.72	330.2	331.7	1.5	552.0	553.5	A $6_1 7_2$
0.00	1060.51	1	2	2	0.50	0.7	351.1	343.0		572.9	564.8	X $7_1 6_1$
2.00	1060.51	1	2	0	2.50	−0.58	351.1			572.9		
1.00	1076.93	0	2	2	0.50	−0.54	367.5			589.3		
1.00	1080.04	0	2	0	1.50	0.5	370.6			592.4		
2.00	1080.09	1	2	0	1.50	0.59	370.7			592.5		
1.00	1110.67	0	2	2	1.50	0.59	401.3			623.1		
3.00	1112.08	0	2	2	2.50	−0.61	402.7			624.5		
1.00	1112.89	0	2	0	0.50	0.6	403.5			625.3		
0.00	1147.86	3	0	0	0.50	0.64	438.5			660.3		
1.00	1155.83	0	4	0	1.50	−0.6	446.4			668.2		
3.00	1158.19	0	4	2	2.50	0.51	448.8			670.6		
1.00	1167.49	0	4	2	0.50	−0.6	458.1			679.9		
1.00	1175.37	0	4	0	0.50	−0.49	466.0			687.8		
3.00	1180.39	0	4	4	2.50	0.71	471.0			692.8		
1.00	1187.57	0	4	2	1.50	−0.62	478.2			700.0		
1.00	1209.85	2	2	−2	1.50	0.56	500.5	502.9	2.4	722.3	724.7	A $6_2 7_2$
0.00	1216.03	1	4	0	0.50	−0.55	506.6	509.6	3.0	728.4	731.4	A $6_1 7_4$
								512.5			734.3	X $7_2 6_1$
2.00	1216.31	1	4	2	2.50	0.57	506.9			728.7		
2.00	1218.41	1	4	2	1.50	−0.56	509.0			730.8		
3.00	1223.25	2	2	0	2.50	0.55	513.9			735.7		
1.00	1225.59	2	2	−2	0.50	−0.52	516.2			738.0		
1.00	1233.32	1	3	3	0.50	−0.64	523.9			745.7		
1.00	1248.75	1	3	3	1.50	0.47	539.4			761.2		
1.00	1254.84	1	3	3	1.50	−0.5	545.4			767.2		
2.00	1266.34	0	3	3	1.50	−0.51	556.9			778.7		
0.00	1268.32	0	3	−1	0.50	0.44	558.9			780.7		
2.00	1271.17	2	3	1	2.50	−0.41	561.8			783.6		
1.00	1272.31	1	3	−1	0.50	0.59	562.9			784.7		
3.00	1281.35	1	3	1	2.50	−0.59	572.0			793.8		
2.00	1302.73	0	3	3	2.50	−0.56	593.3			815.1		
0.00	1306.45	0	3	1	0.50	−0.58	597.1			818.9		
2.00	1307.44	0	3	1	1.50	0.59	598.0			819.8		
0.00	1330.53	1	0	0	0.50	0.72	621.1	623.5	2.4	842.9	845.3	A $6_1 7_0$
								626.8			848.6	A 5_1
								629.3			851.1	
1.00	1340.03	3	1	1	0.50	−0.64	630.6			852.4		
1.00	1340.55	3	1	1	1.50	−0.63	631.2			853.0		
2.00	1345.12	3	0	0	2.50	0.7	635.7			857.5		
2.00	1372.81	3	0	0	1.50	−0.67	663.4			885.2		
2.00	1382.46	2	3	−1	2.50	−0.55	673.1			894.9		
0.00	1394.15	2	3	−3	0.50	−0.57	684.8			906.6		
2.00	1398.24	2	3	−1	1.50	0.55	688.8			910.6		
0.00	1410.32	2	3	3	0.50	0.57	700.9	700.8	−0.1	922.7	922.6	A $6_2 7_3$
								708.2			930	X 4_1

[a]Total vibronic energy.
[b]Largest coefficient in the basis expansion.
[c]Calculated energy relative to $A^2\Pi_{3/2}$.
[d]Observed energy relative to $A^2\Pi_{3/2}$. Calculated by taking the energy difference between the R bandheads of the pump and the probe. The uncertainty is around 2 cm^{-1}.
[e]Residuals = observed−calculated.
[f]Calculated energy relative to $X^2\Pi_{3/2}$.
[g]Observed energy relative to $X^2\Pi_{3/2}$.
[h]Tentative assignment for the levels belonging to the $X^2\Sigma^+$ and $A^2\Pi$ states which were not included in the model.

comprise 50% of the v = 0 basis vector with a slightly higher value for the lower level. When the R–T parameter $|\in|$ is larger than 0.5, the lower potential curve has a negative curvature at the linear geometry versus the bending angle. For some value of the bending angle in a *trans*-bent configuration of the chain (estimated at $\sim 10^\circ$ for C_4H by *ab initio* calculations)[23] one of the two potentials shows a minimum. The height of the barrier suggested from the fit is around 300 cm^{-1}. The

TABLE II. Spectroscopic constants inferred for C_4H in the $A^2\Pi$ state (in cm^{-1}, ϵ is dimensionless). The confidence intervals were estimated by varying each parameter independently so that the rms remained smaller than twice its minimum.

A_{so}	−45.5[a]
ω_6	401.4 ±4.0
ω_7	190.8 ±1.0
ϵ_6	−0.99 ±0.01
ϵ_7	−0.061 ±0.03
ϵ_{67}	−0.105 ±0.01
rms	3.6[b]

[a]Fixed parameter.
[b]rms given for 12 observations.

$^2\Pi_x$ and $^2\Pi_y$ orbitals split in two components on bending of the molecule and gives the potential functions shown in Herzberg[24] (Fig. 4(b), lower plot) for mode ω_6. One of the curvatures in the quadratic term is positive while the other is negative. In such a case, the molecule is qualified as quasilinear relative to the ω_6 vibration. This does not occur for mode ω_7 for which both curvatures are positive.

For $|\epsilon_6| < 0.92$ the highest component in energy of the "split" $^2\Pi_{1/2}v = 0$ level starts to be assigned as $^2\Pi_{1/2}v_6 = 2$. This behavior results from a linear-bent geometry and corresponding symmetries in the C_s point group are indicated on Fig. 7. The feature detected at -117 ± 25 cm^{-1} by photoelectron spectroscopy[9] relative to the ground state, which was attributed to a hot band, matches with the first level listed in Table I, the lower $v = 0$ component, although this was not included in the fitted data.

The lowest modes in energy (lying below the $A^2\Pi$ state) did not vary by more than 20–30 cm^{-1} if the basis set size was increased. This indicates that the basis is complete within the relatively low values of vibrational excitation in the levels recorded experimentally. However, complete convergence of the Hamiltonian matrix could not be achieved because for such a high R–T parameter $\epsilon_6 = -0.99$, the basis set needs to be large (with a single bending mode, it was tested that v_{max} had to be greater than 60–80). Because of hardware memory limitations, convergence of the Hamiltonian could not be reached. A restricted basis set was thus used ($v_{max} = 4$), the main focus of this work being to reproduce the lowest vibrational levels of the $A^2\Pi$ and $X^2\Sigma^+$ electronic states of C_4H. Furthermore, in the current theoretical treatment, the potential energy curve is expanded to a quadratic term only (no anharmonicity is included). The present analysis is thus not completely satisfactory; it however serves the purpose of reproducing the experimental vibrational progression for the two lowest bending modes in the $A^2\Pi$ state, with a small number of variable parameters. Such an unusually large R–T parameter has already been calculated for the BF_2 linear molecule in the excited state (the ground state having a bent geometry), $\epsilon \approx 0.93$ for the degenerate vibrational mode.[25]

Although neither the higher energy ω_5 vibration (C–H bend) nor the "symmetric" stretch ω_4 were taken into consideration the energy levels could be reproduced quite satisfactorily. The calculated levels match the experimental values because the measured levels lie below such vibrations and do not appear to have strong interactions with the modes taken into consideration.

IV. CONCLUSION

A double resonance four-wave mixing approach was used to unambiguously identify the vibronic R–T manifold in the $A^2\Pi$ state of C_4H by pumping on the origin $B^2\Pi - X^2\Sigma^+$ electronic transition. An assignment of the levels was carried out by a R–T analysis, leading to a relatively large ϵ_6 in the ground state for the second lowest bending mode as previously found in the upper state. This study results in the detection of levels located below the $A^2\Pi$ state because of high R–T interaction, as is found for example for C_4D.[8]

ACKNOWLEDGMENTS

The research was supported by the Swiss National Science Foundation (project 200020-124349/1).

[1]M. Guelin, S. Green, and P. Thaddeus, Astrophys. J. **224**, L27 (1978).
[2]J. Cernicharo and M. Guelin, Astron. Astrophys. **309**, L27 (1996).
[3]M. Guelin, J. Cernicharo, M. J. Travers, M. C. McCarthy, C. A. Gottlieb, P. Thaddeus, M. Ohishi, S. Saito, and S. Yamamoto, Astron. Astrophys. **317**, L1 (1997).
[4]C. A. Gottlieb, E. W. Gottlieb, P. Thaddeus, and H. Kawamura, Astrophys. J. **275**, 916 (1983).
[5]M. Guelin, J. Cernicharo, S. Navarro, C. A. Gottlieb, and P. Thaddeus, Astron. Astrophys. **182**, L37 (1987).
[6]S. Yamamoto, S. Saito, M. Guelin, J. Cernicharo, H. Suzuki, and M. Ohishi, Astrophys. J. **323**, L149 (1987).
[7]D. R. Woodward, J. C. Pearson, C. A. Gottlieb, and P. Thaddeus, Astrophys. J. **333**, L29, (1988).
[8]K. Hoshina, H. Kohguchi, Y. Ohshima, and Y. Endo, J. Chem. Phys. **108**, 9 (1998).
[9]J. Zhou, E. Garand, and D. M. Neumark, J. Chem. Phys. **127**, 154320 (2007).
[10]J. F. M. Aarts, Mol. Phys. **35**, 1785 (1978).
[11]J. Tang and S. Saito, J. Chem. Phys. **105**, 8020 (1996).
[12]M. Peric, Mol. Phys. **105**, 59 (2007).
[13]R. Raghunandan, F. J. Mazzotti, R. Chauhan, M. Tulej, and J. P. Maier, J. Phys. Chem. A **113**, 13402 (2009).
[14]H. Linnartz, T. Motylewski, and J. P. Maier, J. Chem. Phys. **109**, 3819 (1998).
[15]F. J. Mazzotti, E. Achkasova, R. Chauhan, M. Tulej, P. P. Radi, and J. P. Maier, Phys. Chem. Chem. Phys. **10**, 136 (2008).
[16]C. M. Western, PGOPHER, a program for simulating rotational structure.See http://pgopher.chm.bris.ac.uk.
[17]R. Chauhan, F. J. Mazzotti, R. Raghunandan, M. Tulej, P. P. Radi, and J. P. Maier, J. Phys. Chem. A **114**, 3329 (2010).
[18]H. Linnartz, T. Motylewski, O. Vaizert, J. P. Maier, A. J. Apponi, M. C. McCarthy, C. A. Gottlieb, and P. Thaddeus, J. Mol. Spectrosc. **197**, 1 (1999).
[19]A. Mitrushchenkov, R. Linguerri, P. Rosmus, and J. P. Maier, Mol. Phys. **107**, 1549 (2009).
[20]K. Hoshina and Y. Endo, J. Chem. Phys. **127**, 184304 (2007).
[21]S-G. He and D. J. Clouthier, J. Chem. Phys **123**, 014316 (2005)
[22]S. Graf, J. Geiss, and S. Leutwyler, J. Chem. Phys. **114**, 4542 (2001).
[23]Unpublished calculations.
[24]G. H. Herzberg, "Electronic Spectra and Electronic Structure of Polyatomic Molecules," in *Molecular Spectra and Molecular Structure* (Van Nostrand Reinhold Inc., New York, 1966), Vol. 3.
[25]R. Tarroni and D. J. Clouthier, J. Chem. Phys. **133**, 064304 (2010).